IEEE Access
Multidisciplinary | Rapid Review | Open Access Journal

Received 1 September 2022, accepted 23 September 2022, date of publication 26 September 2022, date of current version 4 October 2022.

Digital Object Identifier 10.1109/ACCESS.2022.3210125

RESEARCH ARTICLE

An Online VSI Error Parameter Identification Method for Multiphase IM With Non-Sinusoidal Power Supply

SHENG LI, GUANGHUI YANG, (Student Member, IEEE), JIAN ZHANG, AND JIAQIANG YANG, (Senior Member, IEEE)

College of Electrical Engineering, Zhejiang University, West Lake District, Hangzhou 310027, China

Corresponding authors: Jian Zhang (jian_zhang_zju@zju.edu.cn) and Jiaqiang Yang (yjq1998@163.com)

This work was supported in part by the Zhejiang Province Public Welfare Technology Application Research Project, China, under Grant LCZ19E070001.

ABSTRACT Voltage-source-inverter (VSI) nonlinearity compensation is an important scheme for improve motor performance. The traditional off-line method is cumbersome and the compensation effect is poor because it does not simulate the real operation of the motor. To solve this problem, an on-line identification method for compensating multiphase machine based on non-sinusoidal power supply is proposed in this paper. First, a full order air-gap flux observer on harmonic plane was established. Then the voltage error is estimated based on a model reference adaptive system (MRAS) and compensated to the given voltage. In the process of identification, the adaptive law of dead-time voltage is designed, and a feedback gain matrix satisfying Lyapunov stability is also designed. Finally, the feasibility and the effectiveness for harmonic suppression of the proposed method are verified on an experimental platform of a seven-phase induction motor platform.

INDEX TERMS Multiphase induction motor, non-sinusoidal power supply, MRAS, VSI nonlinearity, air-gap flux orientation control (AFOC).

NOMENCLATURE

θ	Rotation angle of the magnetic fields.
ω	Electrical angular velocity.
ψ	Flux linkage.
B_g	Amplitude of flux density.
R, L	Resistance and inductance.
α	Reciprocal of rotor time constant.
p_n	Number of pole pair.
ψ_m	Air-gap flux.
Subscripts	
s, r	Stator and rotor component.
sl	Slip component.
σ	leakage component.
d, q	The axes of a rotation frame of reference by rotor flux orientation control (RFOC).
x, y	The axes of a rotation frame of reference by air-gap flux orientation control (AFOC).

The associate editor coordinating the review of this manuscript and approving it for publication was Mauro Gaggero.

I. INTRODUCTION

Multiphase motor has become a hot research area with the development of modern industrial application. At present, multiphase motor has been used in offshore wind power generation, rail transportation and ship electric propulsion systems and so on [1], [2], [3]. The mainly reason is that, compared with three-phase motors, multiphase motors have the advantages of high reliability, large power density, and more controllable degrees of freedom [4], [5], [6]. At the same time, with the increase of phase number, more inverters are needed to drive the motors.

The VSI nonlinearity problem is always an indispensable part of motor drive control. It is mainly caused by the dead time delay and the voltage drop of the insulated gate bipolar transistor (IGBT). This phenomenon results in that the phase voltage supplied to the motor differs from the given value. Due to the existence of the voltage distortion, the control performance of motor deteriorates, such as: distortionary parameter identification, harmonic current increasing, intensified torque chattering and so on [7], [8], [9]. These adverse effects are particularly significant when the motor is operating at low speed. Therefore, VSI nonlinearity compensation plays a great important part in motor control.

As for multiphase machine studied in this paper, its voltage fluctuations at neutral points are affected by seven-phase currents. It leads to the presence of higher harmonic voltages rather than $(6k \pm 1)$th order harmonic [10]. Third harmonic current injection is widely used in multiphase motor control to improve torque performance [11], [12], [13], [14]. An accurate flux observer is of great help to multiphase motors [14], [15]. However, voltage distortion has non-ignorable influence on flux observer at low speed. Therefore, the given voltage is badly in need of compensation for seven-phase.

At present, the methods of VSI nonlinear compensation can be divided into two categories: off-line measurement compensation and online identification compensation. The off-line compensation method consists of look-up-table (LUT) [16] and fitting curve [8], [17]. This kind of skills is easy to understand but cumbersome in operation and not universal. When the bus voltage or dead time was changed, the off-line compensation method needs to be re-measured. Online compensation methods also mainly include two kinds. One of them is approximates off-line fitting curve compensation [18], [19], [20]. It can adjust the parameters of the fitting function online to achieve that actual voltage is equal to given voltage. However, these method did not take into account voltage fluctuations at neutral points. The other approach is to treat the VSI nonlinearity as a constant times the polarity of the current under synchronous coordinate frame [21], [22], [23]. Then, the constant can be estimated by Low-Pass Filter, Kalman-Filter and current injection [24], [25], [26]. The method proposed in [24] can only used in PMSM $i_d = 0$ control. In [25], the estimated voltage error is fed back only to the observer. It improves the accuracy of the observer, but it has no suppression effect on harmonic currents. Though [26] reduced the harmonic current, additional current injection will increase motor losses.

In this paper, a new VSI nonlinearity parameter identification and compensation algorithm based on non-sinusoidal power supply is proposed. Due to the harmonic injection will provide the extra torque on harmonic plane for the prototype, the advantages of this algorithm are particularly obvious in the multiphase motor we studied. At the same time, by using the degree of freedom of the harmonic plane, the parameters of voltage error can be identified on the harmonic plane with a MRAS and compensated to the given voltage. This identification method is mainly used to estimate speed and other motor parameters [15], [27], [28], [29]. A new adaptive law is designed for inverter voltage error identification. If the feedback gain matrix is not considered during the design process, the adaptive law cannot meet the stability requirement [30]. Therefore a feedback gain matrix satisfying Lyapunov stability is designed in this paper.

The outline of this paper is as follows. In section II, we explained how the nonlinearity of VSI produce and establish the voltage error model of traditional method. Then, we analyzed the shortcomings of the traditional model and establish the VSI model under synchronous coordinate frame. In section III, we built a full-order flux observer for third harmonic plane based on AFOC and identified the voltage error by MRAS method. Moreover, in the process of error voltage adaptive law calculation, we designed a set of feedback gain matrix satisfying Lyapunov's stability. Next, the algorithm is validated on a self-designed seven-phase induction motor experimental platform. Finally, the conclusion is drawn.

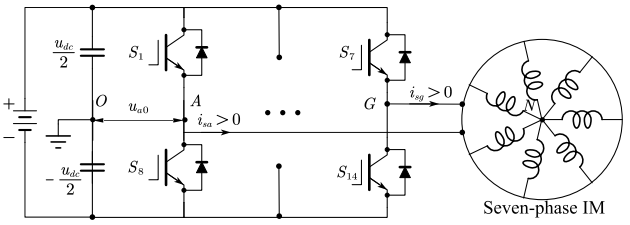

FIGURE 1. Seven-phase IM drive system.

II. OFFLINE COMPENSATION METHOD

A. NONLINEARITY OF VSI MODEL

As shown in Fig.1, the switch signal S_1 is 0 or 1. Take phase A as an example, if $i_{sa} \geqslant 0$ and $S_1 = 1$, the voltage between A and ground is $u_{ao} = \frac{V_{dc}}{2} - V_{sat}$, where V_{sat} is the saturation voltage of the active switch S_1. If $i_{sa} \geqslant 0$ and $S_1 = 0$, $u_{ao} = -\frac{V_{dc}}{2} - V_d$ where, V_d is the forward voltage of the antiparallel diode. In case of $i_{sa} < 0$, the terminal voltage $u_{ao} = \frac{V_{dc}}{2} + V_d$ when $S_1 = 1$. The voltage become $-\frac{V_{dc}}{2} + V_{sat}$ when S_1 turn to 0. In general, the final form of the voltage can be expressed as following [23]:

$$u_{ao} = (V_{dc} - V_{sat} + V_d)\left(S_1 - \frac{1}{2}\right) - \frac{1}{2}(V_{sat} + V_d)\,\mathrm{sgn}(i_{sa}) \tag{1}$$

where sgn (i_{sa}) is the sign function and defined as:

$$\mathrm{sgn}(i_{sa}) = \begin{cases} 1, & i_{sa} > 0 \\ -1, & i_{sa} < 0 \end{cases} \tag{2}$$

In addition, to prevent the short-circuit caused by the upper and lower IGBT in the same leg being turned on at the same time, a dead time delay is usually applied to ensure that the IGBT is completely turned off before the another IGBT in the same leg conduct. Fig.2 (a) displays the reference signal

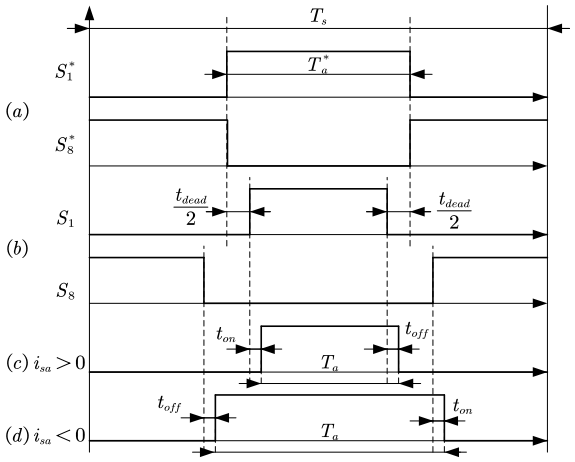

FIGURE 2. Diagram of output voltage waveforms.

of upper and lower IGBT in phase A. After the introduction of dead time, S_1 should be opened later and shut down in advance with $\frac{t_{dead}}{2}$. S_8 need to be shut down later and opened in advance at the same sample time, as shown in Fig.2 (b). In practice, the inverter on and off time needs to be taken into account. When $i_{sa} > 0$, the potential difference waveform between point A and point N in a pulse width modulation (PWM) cycle is shown in Fig.2 (c). Fig.2 (d) shows the voltage waveform under $i_{sa} < 0$.

After considering dead-time effect and IGBT on/off time effect, A-phase voltage is expressed as follows:

$$u_{ao} = (V_{dc} - V_{sat} + V_d)\left(\frac{T_a}{T_s} - \frac{1}{2}\right) - \frac{1}{2}(V_{sat} + V_d)\,\mathrm{sgn}(i_{sa}) \tag{3}$$

where: $T_a = T_a^* - \mathrm{sgn}(i_{sa})\left(t_{dead} + t_{on} - t_{off}\right)$, T_s is the sample time.

B. OFFLINE COMPENSATION METHOD

Usually, a manual measurement of single phase voltage error method is used for feedforward compensating inverter voltage [8], [17]. The method is simple and easy to operate and can meet most industrial needs. The error voltage can be expressed as:

$$u_{aerr} = u_{an}^* - u_{an} \tag{4}$$

The actual voltage of the phase A consists of the resistance voltage, the inductance voltage and the back electromotive force (EMF). The inductance voltage and the back EMF are both zero, because the rotor of the motor is stationary and the injecting current is direct current while using manual measurement method. So the actual voltage of phase A is equal to the voltage drop across the resistance. It is worth noting that since the other phases have no current, the potential at point N is equal to the potential at point O and both are 0. Thus, u_{aerr} can be expressed as:

$$u_{aerr} = u_{an}^* - i_{sa}R_s \tag{5}$$

Fig.3 shows the voltammetry curve after injecting direct current into a single phase. The other curve is the voltammetry curve of error voltage derived from (5). Generally, there are two kinds of off-line feed-forward compensation methods: LUT and curve fitting.

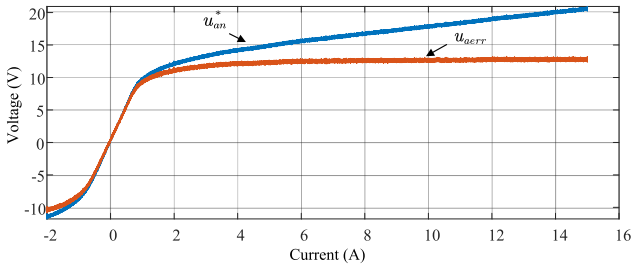

FIGURE 3. Phase voltage and phase voltage error measured with direct current injection.

III. FLUX MODEL OF THIRD HARMONIC PLANE

For the multiphase induction motors, the third harmonic current injection can improve the distribution of the motor air gap flux, so that it could achieve increment of the torque density [31]. Furthermore, there are two mutually independent coordinate planes are formed after PARK transformation with third harmonic current injection. Fortunately, the extra plane can also be used to identity voltage error.

A. HARMONIC CURRENT INJECTION SCHEME

According to the principle of linear superposition, the airgap flux density can be expressed as:

$$B_g(t, \theta_{s1}, \theta_{s3}) = k_1 B_1 \left[\sin(\theta_{s1}) + k_3 \sin(\theta_{s3})\right] \tag{6}$$

where $k_1 = \frac{2}{\sqrt{3}}$ and $k_3 = \frac{1}{6}$ are the optimized proportionality coefficients using genetic algorithm [14], [32].

In order to obtain better flux distribution, this paper adopt a non-sinusoidal power supply control technique which is based on airgap flux orientation [13]. The rms current is reduced by 10.5% when the motor operates at rated load. The given currents on the third harmonic plane are shown in (7a) and (7b):

$$i_{sx3} = \frac{k_1 k_3}{3} \frac{L_{m1}\sqrt{i_{sd1}^2 + \left(1 - \frac{L_{m1}}{L_{r1}}\right)^2 i_{sq1}^2}}{L_{m3}\,(X + Y)} Y \tag{7a}$$

$$i_{sy3} = \frac{k_1 k_3}{3} \frac{L_{m1}\sqrt{i_{sd1}^2 + \left(1 - \frac{L_{m1}}{L_{r1}}\right)^2 i_{sq1}^2}}{L_{m3}\,(X + Y)} \tag{7b}$$

Where:

$$X = -\frac{3\omega_{sl1} L_{r\sigma 3}}{R_{r3}}$$

$$Y = \frac{9\omega_{sl1}^2 L_{r3} L_{r\sigma 3} + R_{r3}^2}{3\omega_{sl1} L_{m3} R_{r3}}$$

B. AIR-GAP FLUX MODEL ON THIRD HARMONIC PLANE

Because of the injection of the third harmonic current, the third harmonic plane is formed which is independent of the fundamental plane. As the harmonic plane is based on airgap flux field orientation, $x-y$ reference frame, its state equation variables should be the currents and the airgap flux, which is shown in:

$$\dot{\boldsymbol{x}}_3 = \boldsymbol{M}_3\boldsymbol{x}_3 + N_3\boldsymbol{u}_3 \tag{8}$$

$$\boldsymbol{y}_3 = \boldsymbol{C}_3\boldsymbol{x}_3 \tag{9}$$

where

$$\boldsymbol{x}_3 = \begin{bmatrix} i_{sx3} & i_{sy3} & \psi_{mx3} & \psi_{my3}, \end{bmatrix}^T$$

$$\boldsymbol{u}_3 = \begin{bmatrix} u_{sx3} & u_{sy3} \end{bmatrix}^T, \quad \boldsymbol{y}_3 = \begin{bmatrix} i_{sx3} & i_{sy3} \end{bmatrix}^T,$$

$$\boldsymbol{M}_3 = \begin{bmatrix} m_{11} & -m_{12} & m_{13} & -m_{14} \\ m_{12} & m_{11} & m_{14} & m_{13} \\ m_{31} & -m_{32} & m_{33} & -m_{34} \\ m_{32} & m_{31} & m_{34} & m_{33} \end{bmatrix},$$

$$N_3 = \begin{bmatrix} n_{11} & 0 \\ 0 & n_{11} \\ n_{31} & 0 \\ 0 & n_{31} \end{bmatrix},$$

$$m_{11} = -\frac{L_{r3}\left(\alpha_3 L_{m3} + R_s\right)}{L_{m3}L_{r\sigma 3} + L_{r3}L_{s\sigma 3}},$$

$$m_{12} = -\frac{L_{m3}L_{r\sigma 3}\left(\omega_{gs3} - \omega_{r3}\right) + \omega_{gs3}L_{r3}L_{s\sigma 3}}{L_{m3}L_{r\sigma 3} + L_{r3}L_{s\sigma 3}},$$

$$m_{13} = \frac{\alpha_3 L_{r3}}{L_{m3}L_{r\sigma 3} + L_{r3}L_{s\sigma 3}}, \quad m_{14} = -\frac{L_{r3}\omega_{r3}}{L_{m3}L_{r\sigma 3} + L_{r3}L_{s\sigma 3}},$$

$$m_{31} = \frac{L_{m3}\left(\alpha_3 L_{r3}L_{s\sigma 3} - L_{r\sigma 3}R_s\right)}{L_{m3}L_{r\sigma 3} + L_{r3}L_{s\sigma 3}},$$

$$m_{32} = -\frac{L_{m3}L_{r\sigma 3}L_{s\sigma 3}\omega_{r3}}{L_{m3}L_{r\sigma 3} + L_{r3}L_{s\sigma 3}},$$

$$m_{33} = -\frac{\alpha_3 L_{r3}L_{s\sigma 3}}{L_{m3}L_{r\sigma 3} + L_{r3}L_{s\sigma 3}},$$

$$m_{34} = -\frac{\omega_{gs3}L_{m3}L_{r\sigma 3} + L_{r3}L_{s\sigma 3}\left(\omega_{gs3} - \omega_{r3}\right)}{L_{m3}L_{r\sigma 3} + L_{r3}L_{s\sigma 3}},$$

$$n_{11} = \frac{L_{r3}}{L_{m3}L_{r\sigma 3} + L_{r3}L_{s\sigma 3}}, \quad n_{31} = \frac{L_{m3}L_{r\sigma 3}}{L_{m3}L_{r\sigma 3} + L_{r3}L_{s\sigma 3}},$$

$$\boldsymbol{C}_3 = \begin{bmatrix} 1 & 0 & 0 & 0 \\ 0 & 1 & 0 & 0 \end{bmatrix}$$

and ω_{gs3} is the synchronous angular velocity of the air-gap flux.

IV. ONLINE COMPENSATION METHOD USING THIRD HARMONIC CURRENT INJECTION

In this section, the extra degrees of freedom on third harmonic plane was used to identity the error of voltage and feedback to the given voltage on synchronous coordinate frame. The whole control block diagram of proposed online method is shown in Fig.4. This method uses MRAS on the third harmonic plane to estimate error voltage. Prior to this, the model VSI nonlinearity on synchronous coordinate frame needs to be rebuilt.

A. VSI NONLINEARITY MODEL ON SYNCHRONOUS COORDINATE FRAME

The offline measurement method is simple, but when the bus voltage or dead zone parameters need to be adjusted, the compensation curve needs to be manually measured off-line again. Moreover, manual measurement method injects direct current into only one phase and assumes that the potential at neutral point N, in Fig.1, is the same as point O. However, when the motor is running normally, the N point potential is affected by the current of each phase [23] and it is not equal to 0.

As shown in Fig.1, after considering the voltage fluctuation of N points, $u_{no} \neq 0$, the actual phase voltage is:

$$u_{an} = u_{ao} - u_{no} \tag{10}$$

The phase voltage of the other phases is expressed in the same way as phase A, which is expressed as following:

$$\begin{bmatrix} u_{bn} \\ \vdots \\ u_{gn} \end{bmatrix} = \begin{bmatrix} u_{bo} \\ \vdots \\ u_{go} \end{bmatrix} - u_{no} \tag{11}$$

In the case of symmetrical and stable operation of the motor, the voltage fluctuation u_{no} can be derived from (10) and (11).

$$u_{no} = \frac{u_{ao} + u_{bo} + u_{co} + u_{do} + u_{eo} + u_{fo} + u_{go}}{7} \tag{12}$$

$$u_{no} = \left(V_{dc} - V_{sat} + V_d\right)\left(\frac{1}{7T_s}\sum_{\chi=a}^{g} T_\chi - \frac{1}{2}\right) - \frac{\left(V_{sat} + V_d\right)}{14}\sum_{\chi=a}^{g}\mathrm{sgn}(i_{s\chi}) \tag{13}$$

Substitute (3) into (12), then (13) can be obtain. According to the given phase voltage: $u_{an}^* = V_{dc}\left(\frac{T_a^*}{T_s} - \frac{1}{2}\right)$ and by combining (5), (10) and (13), the voltage error of phase A inverter can be obtained as (14).

$$u_{aerr} = \left(\frac{\left(V_{dc} - V_{sat} + V_d\right)\left(t_{dead} + t_{on} - t_{off}\right)}{T_s} + \frac{V_{sat} + V_d}{2}\right) \times \left(\mathrm{sgn}(i_{sa}) - \frac{1}{7}\sum_{\chi=a}^{g}\mathrm{sgn}(i_{s\chi})\right) + \frac{\left(V_{sat} - V_d\right)}{V_{dc}}u_{an}^* \tag{14}$$

Due to V_{dc} is much larger than $(V_{sat} - V_d)$, the second term in (14) can be neglected normally [25]. So (14) can be simplified as:

$$u_{aerr} = \frac{u_{err}}{7}\left(6\mathrm{sgn}(i_{sa}) - \mathrm{sgn}(i_{sb}) - \mathrm{sgn}(i_{sc}) - \mathrm{sgn}(i_{sd}) - \mathrm{sgn}(i_{se}) - \mathrm{sgn}(i_{sf}) - \mathrm{sgn}(i_{sg})\right) \tag{15}$$

where:

$$u_{err} \triangleq \left(\frac{\left(V_{dc} - V_{sat} + V_d\right)\left(t_{dead} + t_{on} - t_{off}\right)}{T_s} + \frac{\left(V_{sat} + V_d\right)}{2}\right).$$

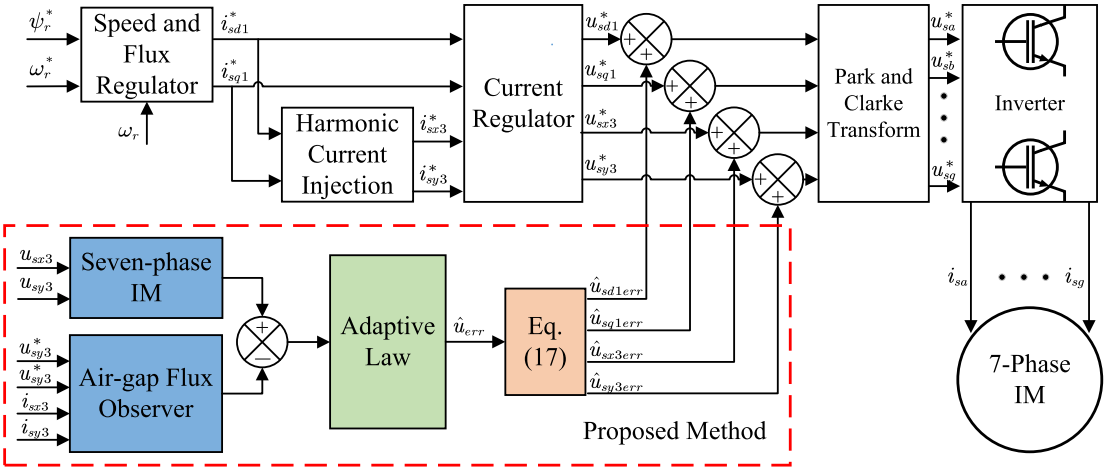

FIGURE 4. Control block diagram of online compensation method.

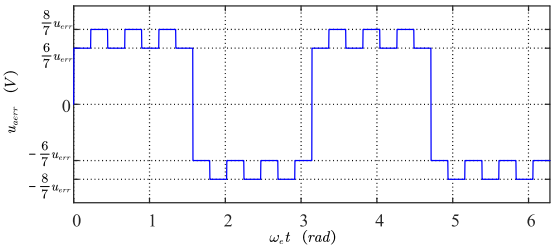

FIGURE 5. Waveform of u_{aerr}.

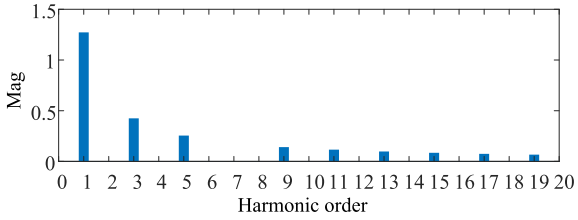

FIGURE 6. FFT results for u_{aerr}.

It can be seen that u_{err} is mainly influenced by V_{dc} and t_{dead}.

According to (15), when seven-phase sinusoidal current is injected into the seven-phase induction motor, the voltage error generated by the inverter of phase A is shown in the Fig.5.

Fig.6 illustrates that VSI nonlinearity will bring $(14k \pm n)$th order harmonic voltage to the system, where k is a non-negative integer, and $n = 1, 3, 5$ [10]. Correspondently, these harmonic voltages produce harmonic currents. Based on the characteristics of the seven-phase motor, the third harmonic and fifth harmonic currents are controllable. So that ninth harmonics, eleventh harmonics and thirteenth harmonics become the main suppression object of inverter compensation algorithm.

The inverter nonlinearity model of seven-phase platform can be extended from (15).

$$\boldsymbol{u}_{err} = u_{err}\boldsymbol{C}_7 \mathrm{sgn}(\boldsymbol{i}_{sab}) \tag{16}$$

where:

$$\boldsymbol{u}_{err} = \begin{bmatrix} u_{aerr} & \cdots & u_{gerr} \end{bmatrix}^T, \quad \boldsymbol{i}_{sab} = \begin{bmatrix} i_{sa} & \cdots & i_{sg} \end{bmatrix}^T,$$

$$\boldsymbol{C}_7 = \frac{1}{7}\begin{bmatrix} 6 & -1 & -1 & -1 & -1 & -1 & -1 \\ -1 & 6 & -1 & -1 & -1 & -1 & -1 \\ -1 & -1 & 6 & -1 & -1 & -1 & -1 \\ -1 & -1 & -1 & 6 & -1 & -1 & -1 \\ -1 & -1 & -1 & -1 & 6 & -1 & -1 \\ -1 & -1 & -1 & -1 & -1 & 6 & -1 \\ -1 & -1 & -1 & -1 & -1 & -1 & 6 \end{bmatrix}.$$

Usually, IMs is analyzed under synchronous rotation frame. Therefore, the VSI nonlinearity model can be calculated from (16).

$$\begin{bmatrix} u_{sd1err} \\ u_{sq1err} \\ u_{sx3err} \\ u_{sy3err} \end{bmatrix} = u_{err} \begin{bmatrix} f_{d1} \\ f_{q1} \\ f_{x3} \\ f_{y3} \end{bmatrix} \tag{17}$$

where:

$$\begin{bmatrix} f_{d1} \\ f_{q1} \\ f_{x3} \\ f_{y3} \end{bmatrix} = \boldsymbol{T}(\theta_{r1}, \theta_{m3}) \begin{bmatrix} \mathrm{sgn}(i_{sa}) \\ \vdots \\ \mathrm{sgn}(i_{sg}) \end{bmatrix}$$

and $\boldsymbol{T}(\theta_{r1}, \theta_{m3})$ is represents the Park transformation. It is noticed that fifth harmonic variables are not listed, because fifth harmonic current was controlled to zero.

B. DESIGN OF ADAPTIVE LAW

Once VSI nonlinearity is taken into consideration, the actual machine model in rotating reference frame on third harmonic plane can be written as:

$$\dot{\boldsymbol{x}}_3 = \boldsymbol{M}_3\boldsymbol{x}_3 + \boldsymbol{N}_3\left(\boldsymbol{u}_3^* - \boldsymbol{u}_{3err}\right) \tag{18}$$

where: $\boldsymbol{u}_3^* = \left[u_{sx3}^* \; u_{sy3}^*\right]^T$, are the given voltage of xy axis respectively on the harmonic plane, $\boldsymbol{u}_{3err} = \left[u_{sx3err} \; u_{sy3err}\right]^T$ are the real error voltage of xy axis.

In fact, the actual error voltage can not be obtained. Thus, u_{err} needs to be estimated. After introducing the estimates, the observer state equation is obtained as follows:

$$\dot{\hat{\boldsymbol{x}}}_3 = \boldsymbol{M}_3\hat{\boldsymbol{x}}_3 + \boldsymbol{N}_3\left(\boldsymbol{u}_3^* - \hat{\boldsymbol{u}}_{3err}\right) + \boldsymbol{G}_3\left(\boldsymbol{y}_3 - \boldsymbol{C}_3\hat{\boldsymbol{x}}_3\right) \quad (19)$$

where $\boldsymbol{G}_3$ is the feedback gain matrix.

Substituting the estimation parameters into the observer state equation and error state equation can be obtained.

$$\dot{\boldsymbol{e}}_3 = \left(\boldsymbol{M}_3 - \boldsymbol{G}_3\boldsymbol{C}_3\right)\boldsymbol{e}_3 - \boldsymbol{N}_3\Delta\boldsymbol{u}_{3err} \quad (20)$$

where: $\boldsymbol{e}_3 = \boldsymbol{x}_3 - \hat{\boldsymbol{x}}_3$, $\Delta\boldsymbol{u}_{3err} = \Delta u_{err}\left[f_{x3} \; f_{y3}\right]^T$ $\Delta u_{err} = u_{err} - \hat{u}_{err}$.

A positive definite Lyapunov function which is containing parameter error space can be constructed [27], [28], [30]:

$$V = \frac{1}{2}\boldsymbol{e}^T\boldsymbol{P}\boldsymbol{e} + \frac{\lambda_u}{2}\left(u_{err} - \hat{u}_{err}\right)^2 \qquad \boldsymbol{P} \in \boldsymbol{R}^{4\times4} \quad (21)$$

where: $\boldsymbol{P}$ is a symmetric positive definite matrix.

The derivative of the Lyapunov function (21) becomes:

$$\dot{V} = \frac{1}{2}\boldsymbol{e}^T\left(\left(\boldsymbol{M}_3 - \boldsymbol{G}_3\boldsymbol{C}_1\right)^T\boldsymbol{P} + \boldsymbol{P}\left(\boldsymbol{M}_3 - \boldsymbol{G}_3\boldsymbol{C}_1\right)\right)\boldsymbol{e} - \boldsymbol{e}^T\boldsymbol{P}\boldsymbol{N}_3\Delta\boldsymbol{u}_{err} - \lambda_u\Delta u_{err}\frac{d\hat{u}_{err}}{dt} \quad (22)$$

According to the Lyapunov stability theorem, a sufficient condition for the asymptotic stability of the estimator is that the candidate function V must be decreased while the error is not zero [28], [30]. Therefore, the first-order time derivative of (21) must be negative when $\boldsymbol{e} \neq 0$. ${\boldsymbol{M}_{3g}}^T\boldsymbol{P} + \boldsymbol{P}\boldsymbol{M}_{3g}$ can be guaranteed to be negative definite matrix through the design of $\boldsymbol{G}_3$ and $\boldsymbol{P}$ ($\boldsymbol{M}_{3g} = \boldsymbol{M}_3 - \boldsymbol{G}_3\boldsymbol{C}_1$). Generally, $\boldsymbol{P}$ is assumed to be the identity matrix, so that the gain matrix needs to be designed which will be discussed in the next part. If the gain matrix is properly designed, the Lyapunov condition will eventually be satisfied, if the sum of the last two terms in (22) is zero as:

$$-\boldsymbol{e}^T\boldsymbol{P}\boldsymbol{N}_3\Delta\boldsymbol{u}_{err} - \lambda_u\Delta u_{err}\frac{d\hat{u}_{err}}{dt} = 0 \quad (23)$$

Since the flux can not be measured, the estimated error of the flux can be ignored, which would not affect the stability in practice [29]. By substituting (17), into (23), the adaptation law can be described by:

$$\frac{d\hat{u}_{err}}{dt} = -\frac{L_{r3}\left(e_{isx3}f_{x3} + e_{isy3}f_{y3}\right)}{\lambda_u\left(L_{m3}L_{r\sigma3} + L_{r3}L_{s\sigma3}\right)} \quad (24)$$

C. DESIGN OF GAIN MATRIX

If the feedback gain matrix is not designed, the coefficient matrix of the first term in (22) cannot be guaranteed to be a negative definite matrix. It means that the above adaptive law (24) cannot satisfy the asymptotic stability defined by Lyapunov. Therefore, the gain matrix need to be designed according to Lyapunov theory. The design of feedback matrix becomes the requirement of this paper.

$$\boldsymbol{G}_3 = \begin{bmatrix} g_1 & g_2 & g_3 & g_4 \\ -g_2 & g_1 & -g_4 & g_3 \end{bmatrix}^T \quad (25)$$

We assumed that:

$${\boldsymbol{M}_{3g}}^T\boldsymbol{P} + \boldsymbol{P}\boldsymbol{M}_{3g} = \boldsymbol{Q} \quad (26)$$

Obviously, is a fourth order real symmetric matrix. $|\boldsymbol{Q}_n|$ represents leading principal minor of $\boldsymbol{Q}$, where $n = 1, 2, 3, 4$. Substituting (25) into (26) can we obtain:

$$|\boldsymbol{Q}_1| = 2\left(m_{11} - g_1\right) \quad (27a)$$

$$|\boldsymbol{Q}_2| = 4\left(m_{11} - g_1\right)^2 \quad (27b)$$

$$|\boldsymbol{Q}_3| = 2\left(m_{11} - g_1\right)\left(4\left(m_{11} - g_1\right)m_{33} - \left(m_{13}+m_{31}-g_3\right)^2 - \left(m_{32}-m_{14}-g_4\right)^2\right) \quad (27c)$$

$$|\boldsymbol{Q}_4| = \left(4\left(m_{11}-g_1\right)m_{33} - \left(m_{13}+m_{31}-g_3\right)^2 - \left(m_{32}-m_{14}-g_4\right)^2\right)^2 \quad (27d)$$

In order to the satisfy Lyapunov stability theorem, $\boldsymbol{Q}_3$ must be a negative definite matrix. $\boldsymbol{G}_3$, a necessary not sufficient condition for the stability is easy to be designed as:

$$\begin{aligned} g_1 &= 2\delta \\ g_2 &= 0 \\ g_3 &= m_{13} + m_{31} \\ g_4 &= m_{32} - m_{14} \end{aligned}$$

where $\delta > 0$.

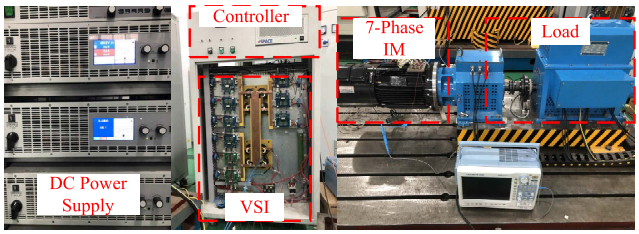

FIGURE 7. Seven-phase experimental system.

V. EXPERIMENT AND EVALUATION

A. EXPERIMENTAL SYSTEM SETUP

The proposed algorithm is validated on a seven-phase induction motor experimental platform. Fig.7 displays the complete experimental platform, which is composed of DC power supply, dSPACE-1005 controller, multiphase VSI and alternating current servo load. The multi-phase VSI is constructed by several groups of IGBT device, filter capacitors, current and voltage sensors, etc. In particular, the IGBT model is the INFINEON FF150R12ME3G. The sampling frequency of the platform is 10 kHz, and the dead time is set to 3 μs to ensure the safety of the system. Table 1 and Table 2 exhibit all parameters of the self-designed squirrel-cage seven-phase induction motor.

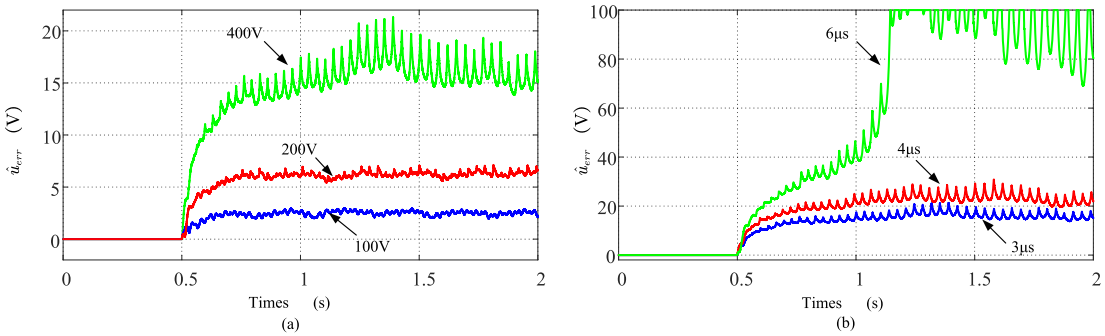

FIGURE 8. Identification process of traditional method: (a) different V_{dc} under $t_{dead} = 3\mu s$. (b)different t_{dead} under $V_{dc} = 400V$.

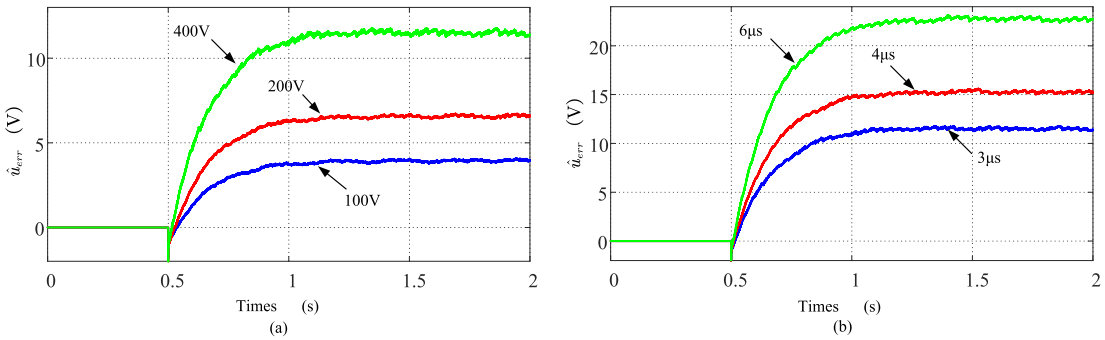

FIGURE 9. Identification process of proposed method: (a) different V_{dc} under $t_{dead} = 3\mu s$. (b)different t_{dead} under $V_{dc} = 400V$.

TABLE 1. Main parameters of the prototype.

Parameters category	Notation	Value
Pole pair number	p_n	2
Rated voltage (RMS)	-	110 V
Rated current (RMS)	-	8.5 A
Rated speed	-	1460 rpm
Rated torque	-	35 N·m

TABLE 2. Parameters of each plane.

Parameters category	1^{st}plane	3^{rd}plane	5^{th}plane
Magnetizing inductance	129.8 mH	15.3 mH	5.9 mH
Stator leakage inductance	6.5 mH	4.2 mH	3.9 mH
Rotor leakage inductance	6.0 mH	3.5 mH	3.2 mH
Stator resistance	0.51 Ω	0.51 Ω	0.51 Ω
Rotor resistance	0.39 Ω	0.33 Ω	0.31 Ω

B. COMPARISON OF ONLINE ADAPTIVE METHODS

If the motor is running at high speed, the phase voltage of the motor is very large. At this point, the voltage distortion generated by the VSI has little effect on motor performance, or even can be ignored. However, when the motor speed is lower, the dead-time effect is more obvious. Thus, all experiments were carried out at 2% of rated speed.

In order to verify the superiority of the proposed method in parameter identification performance, the proposed method is compared with the traditional MRAS method which is described in detail in the Appendix. The seven-phase machine runs steadily at 30 rpm and rated-load condition. The algorithm starts at 0.5 s. Fig.8 (a) exhibits that u_{err} estimated by traditional method can converge to 6.34 V and 2.49 V when the bus voltage is set 200 V and 100 V respectively. When the bus voltage up to 400 V, traditional method has poor performance. It can not converge to a constant. At $V_{dc} =$ 400 V, when the deadtime is set to 6 μs, the system crashed after 1 second, which is illustrated in Fig.8 (b).

However, the proposed method can operate stably under all the above conditions and can converge stably to a constant. In Fig.9 (a), the estimated error voltage converges to 3.95 V when the bus voltage is 100 V. When V_{dc} increase to 200 V, 400 V respectively, $\hat{u}_{err}$ become 6.54 V and 11.52 V after 1 s. In Fig.9 (b), it can be seen that when t_{dead} is adjusted to 4 μs and 6 μs under $V_{dc} = 400$ V, estimated value of voltage error converge to 15.25 V and 22.72 V correspondingly.

TABLE 3. Comparison of reference value and estimates.

Bus Voltage and Dead Time		Reference Value	Estimated Value	Estimate Deviation
3 μs	100 V	4.28 V	3.95 V	7.7%
	200 V	6.88 V	6.54 V	4.9%
	400 V	12.08 V	11.52 V	4.6%
400 V	3 μs	12.08 V	11.52 V	4.6%
	4 μs	16.08 V	15.25 V	5.1%
	6 μs	24.08 V	22.72 V	5.6%

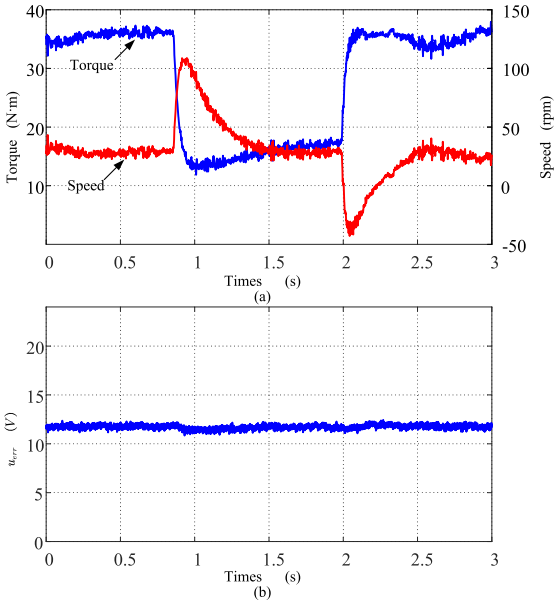

FIGURE 10. Estimated value with load variation: (a) Load and speed curve. (b) Estimated value curve.

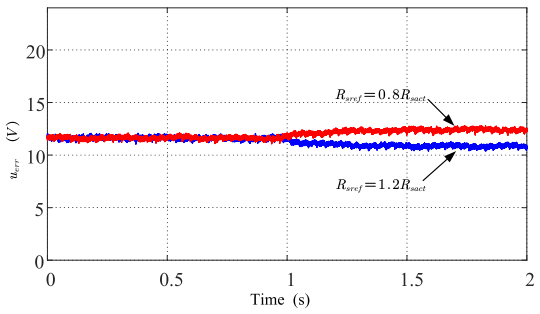

FIGURE 11. Estimated value with R_{sref} variation.

According to the IGBT parameters from data sheet, the reference value of u_{err} can be calculated, which is list in Table 3. It can be seen that, under above conditions, the deviation between the estimated value and the reference value is about 5%. The errors are sufficient for most industry applications. Therefore, the evaluation of the proposed method is reliable.

C. ESTIMATE OF $\hat{u}_{err}$ AT VARIOUS CONDITIONS

During the actual operation, the system load is usually changed. In order to test the performance of the proposed algorithm in practical applications, the load variation experiments are given in Fig.10. Fig.10 (a) shows the running state of the motor. The load is reduced to half at around 0.8 s and increased to full load at 2 s. The motor speed also varies with the load. However, the VSI nonlinear identified by the proposed method does not change much. The fluctuation factor of $\hat{u}_{err}$ is 5.1% which is shown as Fig.10 (b).

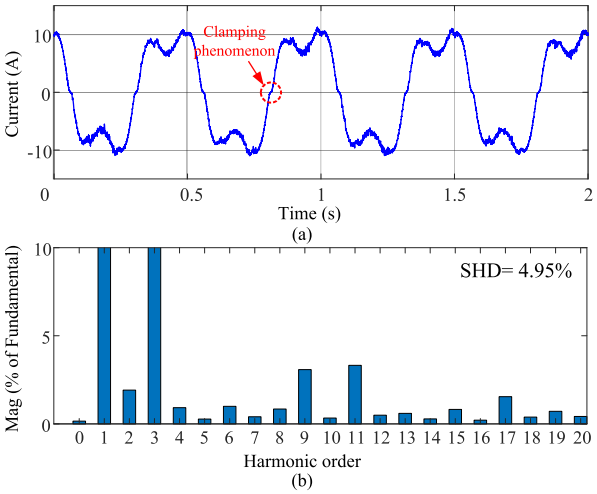

FIGURE 12. FFT results for output currents of no compensation at 30 rpm and rated load. (a) output current of phase A. (b) FFT results.

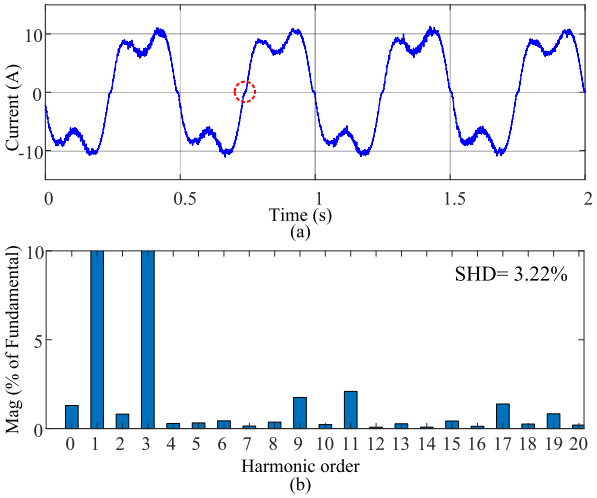

FIGURE 13. FFT results for output currents of off-line compensation at 30 rpm and rated load. (a) output current of phase A. (b) FFT results.

As we all know, the long-term operation will result in the temperature increasing of the motor and the winding resistance will change. Therefore, this paper also shows the performance of the proposed algorithm when the actual parameters of the motor deviate from the control parameters. Fig.11 shows the VSI error identification curve when resistance deviation occurs in the proposed method. In Fig.11, R_{sref} is the reference in the control system, and R_{sact} is the actual value. When the reference resistance is 20% greater than the actual resistance, the estimate of u_{err} will be an about 6.5% reduction. Otherwise, when the reference resistance is 20% smaller than the actual resistance, the estimate of u_{err} will rise about 6.7%. It can be seen that the proposed method is affected by the variation of motor parameters. The reason is that the proposed method is based on the model of the air-gap flux observer. When the model itself has errors, the parameter identification results will also produce errors.

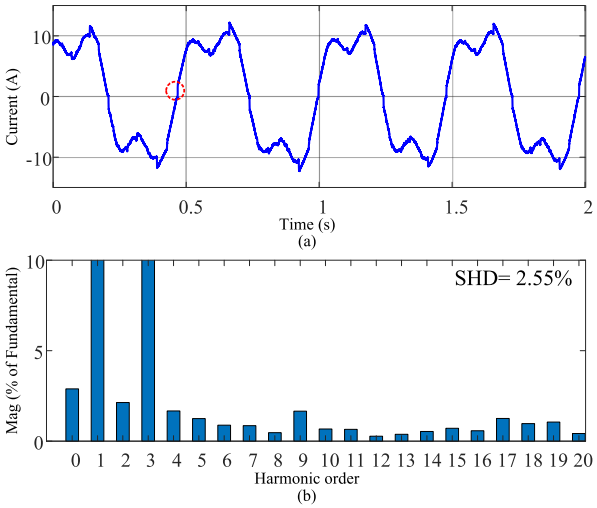

FIGURE 14. FFT results for output currents of traditional MRAS compensation at 30 rpm and rated load. (a) output current of phase A. (b) FFT results.

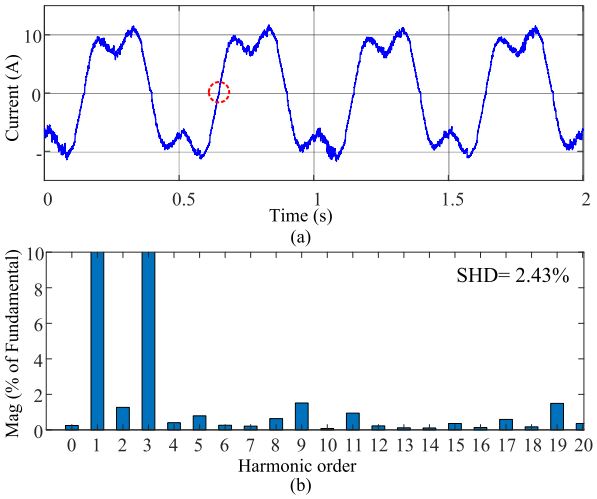

FIGURE 15. FFT results for output currents of proposed on-line compensation at 30 rpm and rated load. (a) output current of phase A. (b) FFT results.

D. COMPARATIVE EXPERIMENT OF COMPENSATION EFFECT

The dead-time effect of seven-phase IGBTs mainly produce $(14\pm n)$th order harmonic current. Therefore, the performance of proposed method is mainly reflected in the suppression of these harmonics. As third harmonic is injected actively, third harmonic would be much larger than other harmonics. It leads to the the value of total harmonic distortion (THD) can not reflect the advantage of the algorithm. Thus, a selective harmonic distortions (SHD) was adopted, which is defined as:

$$\mathrm{SHD}\,[\%] = \frac{\sqrt{I_9^2 + I_{11}^2 + I_{13}^2 + I_{15}^2 + I_{17}^2 + I_{19}^2}}{I_1} \tag{28}$$

where I_k is the magnitude of the kth order harmonic [33].

In Fig.12, Fig.13, Fig.14 and Fig.15 the prototype was operated with a rated load and 30 rpm. The bus voltage is 400 V, and dead time is adjusted to 3 μs. Fig.12 (a) displays the current of phase A without using any VSI nonlinearity compensation. It can be seen that the current has obvious distortion near zero point which is caused by the inverter dead-time effect. After FFT analysis of the current, the SHD = 4.95% when there is no compensation for the drive system as shown in Fig.12 (b). It is worth noting that the 9th and 11th order harmonics dominate. These high order harmonics increase the loss of the motor and greatly harm the performance of the motor.

As for Fig.13 (a), when the offline feedforward method was adopted, the current distortion has been little improved on the zero crossing point. The value of SHD decrease to 3.22%, which is shown as Fig.13 (b). Among them, there has been a noticeable decrease in 9th and 11th order harmonics. In Fig.14, after using the traditional MRAS method, as the compensation voltage is higher than the required voltage, the zero crossing of the current curve is not smooth. Fortunately, its SHD decrease to 2.55%. The zero current clamping phenomenon is almost eliminated which is shown as Fig.15 (a). Moreover, the harmonic content decreases more significantly, SHD = 2.43%. These experiments are enough to conclude that the proposed method not only can adapt to various operating conditions, but also has obvious advantages in harmonic suppression.

VI. CONCLUSION

Non-sinusoidal power supply is a significant application for multiphase motors. In this paper, a VSI nonlinearity identification method based on third harmonic injection is proposed. In addition, this method utilizes third harmonic plane only, and the fundamental plane can be used for other parameter estimation purposes. In order to make the adaptive law of voltage error stable, we designed a feedback gain matrix of a full-order air-gap flux observer. Based on the above algorithm, a series of experiments are carried out on a seven-phase induction motor. By comparing the estimated values with the reference values which is calculated from IGBT data sheet, the errors are satisfactory under different conditions. It is important to note that the accuracy of the estimates is affected by parameters of the flux observer, especially the stator resistance. Finally, the proposed method can not only estimate the reliable voltage error of the inverter, but also effectively reduce the SHD.

APPENDIX

In this Appendix, the traditional VSI nonlinearity estimation method mentioned in the experiment is given [22], [23]. In [22], the authors obtained the VSI error by direct calculation which is expressed as:

$$u_{err} = \frac{u^*_{sy3} - u_{sy3}}{f_y} \tag{A1}$$

The actual voltage of the motor can be calculated from the flux equation and voltage equation. Then, (A1) can be

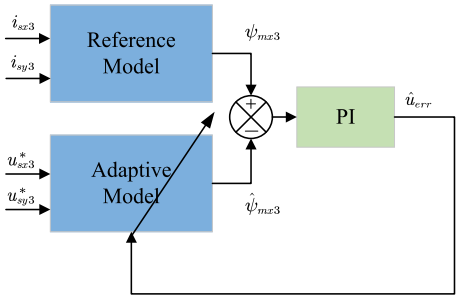

FIGURE 16. Block diagram of traditional MRAS method.

changed to:

$$\hat{u}_{err} = \frac{u^*_{sy3} - R_s i_{sy3} - L_{s3} i_{sx3} \omega_{gs3}}{f_y} - \frac{L_{m3} L_{r\sigma 3} \left(\omega_{r3} - \omega_{gs3}\right)}{\alpha_3 L_{r3} f_y} \omega_{gs3} i_{sy3} \quad \text{(A2)}$$

The denominator of (A2) contains f_y, and f_y is close to zero, so that the perturbation of f_y is going to be amplified in the estimation. A low pass filter is used to reduce this disturbance [22], but the effect is not obvious. Therefore, after two years, they optimized the perturbation of the estimated value by using MRAS [23]. As for the induction machine in this article, there are two types of air-gap flux observer, voltage model and current model. For the current model does not contain voltage variables, it is used as the reference model.

$$\psi_{mx3} = L_{m3} i_{sx3} + \frac{L_{m3} L_{r\sigma 3} \left(\omega_{r3} - \omega_{gs3}\right)}{\alpha_3 L_{r3}} i_{sy3} \quad \text{(A3)}$$

On the other hand, voltage model is regarded as adaptive model which is expressed as (A4). It is noticed that these two models are steady-state mathematical models of air-gap flux.

$$\hat{\psi}_{mx3} = \frac{u^*_{sy3} - \hat{u}_{err} f_{y3} - R_s i_{sy3}}{\omega_{gs3}} - L_{s\sigma 3} i_{sx3} \quad \text{(A4)}$$

The u_{err} can be estimated by the error of the two air-gap fluxes.

$$\hat{u}_{err} = \frac{k_p s + k_i}{s} \left(\psi_{mx3} - \hat{\psi}_{mx3}\right) \quad \text{(A5)}$$

Fig.16 shows the block diagram of traditional MRAS method.

REFERENCES

[1] E. Levi, R. Bojoi, F. Profumo, H. A. Toliyat, and S. Williamson, "Multiphase induction motor drives—A technology status review," *IET Electr. Power Appl.*, vol. 1, no. 4, p. 489, 2007.

[2] E. Levi, "Multiphase electric machines for variable-speed applications," *IEEE Trans. Ind. Electron.*, vol. 55, no. 5, pp. 1893–1909, May 2008.

[3] E. Levi, F. Barrero, and M. J. Duran, "Multiphase machines and drives—Revisited," *IEEE Trans. Ind. Electron.*, vol. 63, no. 1, pp. 429–432, Jan. 2016.

[4] J. Sun, Z. Liu, Z. Zheng, and Y. Li, "An online global fault-tolerant control strategy for symmetrical multiphase machines with minimum losses in full torque production range," *IEEE Trans. Power Electron.*, vol. 35, no. 3, pp. 2819–2830, Mar. 2020.

[5] Y. Wang, J. Yang, and J. Gao, "Non-sinusoidal supply control strategy based on rotor and air-gap flux orientation for multiphase induction machine," in *Proc. 22nd Int. Conf. Electr. Mach. Syst. (ICEMS)*, Aug. 2019, pp. 1–6.

[6] G. Yang, J. Yang, S. Li, Y. Wang, H. Hussain, L. Yan, and R. Deng, "Overmodulation strategy for seven-phase induction motors with optimum harmonic voltage injection based on sequential optimization scheme," *IEEE Trans. Power Electron.*, vol. 36, no. 12, pp. 14039–14050, Dec. 2021.

[7] W. Sun, J. Gao, X. Liu, Y. Yu, G. Wang, and D. Xu, "Inverter nonlinear error compensation using feedback gains and self-tuning estimated current error in adaptive full-order observer," *IEEE Trans. Ind. Appl.*, vol. 52, no. 1, pp. 472–482, Jan. 2016.

[8] Y. Wang, J. Yang, S. Li, G. Yang, R. Deng, and H. Hussain, "Multiplane rotor resistance online estimation strategy for multiphase induction machine under nonsinusoidal power supply," *IEEE Trans. Power Electron.*, vol. 36, no. 8, pp. 9487–9500, Aug. 2021.

[9] N. Bedetti, S. Calligaro, and R. Petrella, "Self-commissioning of inverter dead-time compensation by multiple linear regression based on a physical model," *IEEE Trans. Ind. Appl.*, vol. 51, no. 5, pp. 3954–3964, Sep. 2015.

[10] W. Dong, W. Xin-Zhen, M. Wei-Ming, W. Xin-Lu, and G. Yun-Jun, "Air-gap MMF analysis of fifteen-phase induction motor with non-sinusoidal supply," *Proc. CSEE*, vol. 29, no. 15, pp. 88–94, 2009.

[11] L. Zheng, J. E. Fletcher, B. W. Williams, and X. He, "Dual-plane vector control of a five-phase induction machine for an improved flux pattern," *IEEE Trans. Ind. Electron.*, vol. 55, no. 5, pp. 1996–2005, May 2008.

[12] A. S. Abdel-Khalik, M. I. Masoud, and B. W. Williams, "Improved flux pattern with third harmonic injection for multiphase induction machines," *IEEE Trans. Power Electron.*, vol. 27, no. 3, pp. 1563–1578, Mar. 2012.

[13] Y. Wang, J. Yang, G. Yang, S. Li, and R. Deng, "Harmonic currents injection strategy with optimal air gap flux distribution for multiphase induction machine," *IEEE Trans. Power Electron.*, vol. 36, no. 1, pp. 1054–1064, Jan. 2021.

[14] S. Li, G. Yang, Y. Wang, and J. Yang, "Dual closed-loop control strategy on harmonic plane for multiphase induction motor with harmonic injection based on air-gap flux orientation control," *IEEE J. Emerg. Sel. Topics Power Electron.*, early access, Feb. 24, 2022, doi: 10.1109/JESTPE.2022.3154427.

[15] S. Li, J. Yang, Y. Wang, G. Yang, T. Gu, S. Q. Zhuo, and F. Li, "Sensorless control strategy for multiphase induction motor with stator and rotor resistance identification based on injecting third harmonic current," in *Proc. IEEE 1st China Int. Youth Conf. Electr. Eng. (CIYCEE)*, Nov. 2020, pp. 1–7.

[16] G. Pellegrino, R. I. Bojoi, P. Guglielmi, and F. Cupertino, "Accurate inverter error compensation and related self-commissioning scheme in sensorless induction motor drives," *IEEE Trans. Ind. Appl.*, vol. 46, no. 5, pp. 1970–1978, Sep. 2010.

[17] G. Shen, W. Yao, B. Chen, K. Wang, K. Lee, and Z. Lu, "Automeasurement of the inverter output voltage delay curve to compensate for inverter nonlinearity in sensorless motor drives," *IEEE Trans. Power Electron.*, vol. 29, no. 10, pp. 5542–5553, Oct. 2014.

[18] W. Yang, Y. Wang, L. Yan, Z. Han, and D. Gerling, "Online detection of inverter voltage error based on the voltage oversampling measurement and sigmoidal function model," *IEEE Trans. Power Electron.*, vol. 37, no. 1, pp. 303–312, Jan. 2022.

[19] X. Yuan, J. Chen, Y. Zuo, and C. H. T. Lee, "Deadbeat predictive current control considering inverter nonlinearity for permanent magnet synchronous machine drives," in *Proc. IEEE Energy Convers. Congr. Expo. (ECCE)*, Oct. 2021, pp. 4955–4960.

[20] J. Chen, J. Mei, X. Yuan, Y. Zuo, J. Zhu, and C. H. T. Lee, "Online adaptation of two-parameter inverter model in sensorless motor drives," *IEEE Trans. Ind. Electron.*, vol. 69, no. 10, pp. 9860–9871, Oct. 2022.

[21] H.-S. Kim, H.-T. Moon, and M.-J. Youn, "On-line dead-time compensation method using disturbance observer," *IEEE Trans. Power Electron.*, vol. 18, no. 6, pp. 1336–1345, Nov. 2003.

[22] H.-W. Kim, H.-S. Kim, M.-J. Youn, and K.-Y. Cho, "Online observation and compensation of voltage distortion in PWM VSI for PMSM," *IEE Proc.-Electr. Power Appl.*, vol. 151, no. 5, p. 534, 2004.

[23] H.-W. Kim, M.-J. Youn, K.-Y. Cho, and H.-S. Kim, "Nonlinearity estimation and compensation of PWM VSI for PMSM under resistance and flux linkage uncertainty," *IEEE Trans. Control Syst. Technol.*, vol. 14, no. 4, pp. 589–601, Jul. 2006.

[24] D. Liang, J. Li, R. Qu, and W. Kong, "Adaptive second-order sliding-mode observer for PMSM sensorless control considering VSI nonlinearity," *IEEE Trans. Power Electron.*, vol. 33, no. 10, pp. 8994–9004, Oct. 2018.

[25] X. Li and R. Kennel, "General formulation of Kalman-filter-based online parameter identification methods for VSI-fed PMSM," *IEEE Trans. Ind. Electron.*, vol. 68, no. 4, pp. 2856–2864, Apr. 2021.
[26] K. Yu and Z. Wang, "An online compensation method of VSI nonlinearity for dual three-phase PMSM drives using current injection," *IEEE Trans. Power Electron.*, vol. 37, no. 4, pp. 3769–3774, Apr. 2022.
[27] S. Suwankawin and S. Sangwongwanich, "Design strategy of an adaptive full-order observer for speed-sensorless induction-motor drives-tracking performance and stabilization," *IEEE Trans. Ind. Electron.*, vol. 53, no. 1, pp. 96–119, Feb. 2006.
[28] M. H. Holakooie, M. Ojaghi, and A. Taheri, "Direct torque control of six-phase induction motor with a novel MRAS-based stator resistance estimator," *IEEE Trans. Ind. Electron.*, vol. 65, no. 10, pp. 7685–7696, Oct. 2018.
[29] J. Chen and J. Huang, "Online decoupled stator and rotor resistances adaptation for speed sensorless induction motor drives by a time-division approach," *IEEE Trans. Power Electron.*, vol. 32, no. 6, pp. 4587–4599, Jun. 2017.
[30] L. Harnefors and M. Hinkkanen, "Complete stability of reduced-order and full-order observers for sensorless IM drives," *IEEE Trans. Ind. Electron.*, vol. 55, no. 3, pp. 1319–1329, Mar. 2008.
[31] A. Abdelkhalik, M. Masoud, and W. Barry, "Eleven-phase induction machine: Steady-state analysis and performance evaluation with harmonic injection," *IET Electr. Power Appl.*, vol. 4, no. 8, p. 670, 2010.
[32] A. Abdel-Khalik, M. I. Masoud, S. M. Gadoue, and B. W. Williams, "Optimum flux distribution with harmonic injection for a multiphase induction machine using genetic algorithms," *IEEE Trans. Energy Convers.*, vol. 26, no. 2, pp. 501–512, Jun. 2011.
[33] Y. Park and S.-K. Sul, "A novel method utilizing trapezoidal voltage to compensate for inverter nonlinearity," *IEEE Trans. Power Electron.*, vol. 27, no. 12, pp. 4837–4846, Dec. 2012.

SHENG LI was born in Shanxi, China, in 1994. He received the M.Sc. degree in vehicle engineering from South China Agricultural University, Guangdong, China, in 2018. He is currently pursuing the Ph.D. degree in electrical engineering with the College of Electrical Engineering, Zhejiang University, Hangzhou, China.

His current research interests include advanced control technology for multiphase machines and the machine parameter estimation.

GUANGHUI YANG (Student Member, IEEE) was born in Shanxi, China, in 1997. He received the B.Sc. degree in electrical engineering from Southeast University, Nanjing, China, in 2019. He is currently pursuing the Ph.D. degree in electrical engineering with the College of Electrical Engineering, Zhejiang University, Hangzhou, China.

His current research interests include multiphase induction motor and multiphase inverter control technology.

JIAN ZHANG received the Ph.D. degree in mechanical engineering from Zhejiang University, Hangzhou, China, in 2010. He is currently an Associate Professor of electrical engineering with Zhejiang University. His current research interests include design, control and reliability analysis of electrical machines.

JIAQIANG YANG (Senior Member, IEEE) was born in Jiangsu, China, in 1970. He received the Ph.D. degree in electrical engineering from Zhejiang University, Hangzhou, China, in 2004.

Since 2004, he has been a Lecturer, an Associate Professor, and a Professor with the College of Electrical Engineering, Zhejiang University. From 2012 to 2013, he was a Research Fellow with the College of Electrical and Computer, National University of Singapore, Singapore. His research interests include active power filters, flywheel energy storage systems, and the design and control of motor for electrical vehicle.